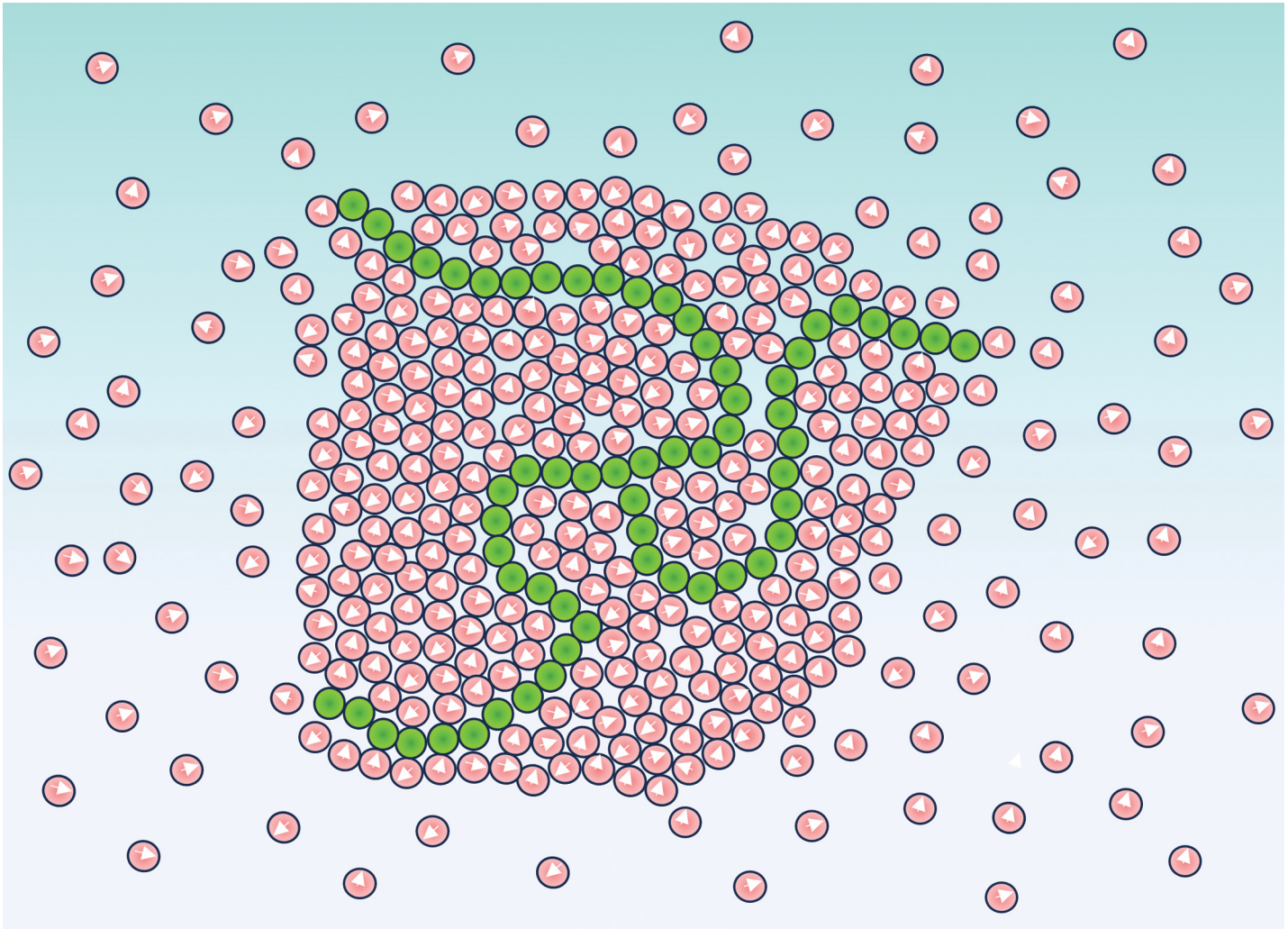

Showcasing research from Professor Rajarshi Chakrabarti's group, Department of Chemistry, Indian Institute of Technology Bombay, India in collaboration with Prof. Ralf Metzler from University of Potsdam, Germany.

A passive star polymer in a dense active bath: insights from computer simulations

Computer simulations illustrate the role of a passive star polymer, immersed in a dense active bath, in regulating the kinetics of the motility induced phase separation (MIPS) and the effect of bath particles on the conformation and dynamics of the star polymer.

As featured in:

See Ralf Metzler, Rajarshi Chakrabarti *et al.*, *Soft Matter*, 2024, **20**, 3910.

ROYAL SOCIETY OF CHEMISTRY

rsc.li/soft-matter-journal

Registered charity number: 207890

Soft Matter

PAPER

View Article Online
View Journal | View Issue

Cite this: *Soft Matter*, 2024, **20**, 3910

A passive star polymer in a dense active bath: insights from computer simulations†

Ramanand Singh Yadav,[a] Sanaa Sharma,[a] Ralf Metzler *[bc] and Rajarshi Chakrabarti *[a]

Using computer simulations in two dimensions (2D), we explore the structure and dynamics of a star polymer with three arms made of passive monomers immersed in a bath of active Brownian particles (ABPs). We analyze the conformational and dynamical changes of the polymer as a function of activity and packing fraction. We also study the process of motility induced phase separation (MIPS) in the presence of a star polymer, which acts as a mobile nucleation center. The presence of the polymer increases the growth rate of the clusters in comparison to a bath without the polymer. In particular, for low packing fraction, both nucleation and cluster growth are affected by the inclusion of the star polymer. Clusters grow in the vicinity of the star polymer, resulting in the star polymer experiencing a caged motion similar to a tagged ABP in the dense phase. Due to the topological constraints of the star polymers and clustering nearby, the conformational changes of the star polymer lead to interesting observations. *Inter alia*, we observe the shrinking of the arm with increasing activity along with a short-lived hairpin structure of one arm formed. We also see the transient pairing of two arms of the star polymer, while the third is largely separated at high activity. We hope our findings will help in understanding the behavior of active–passive mixtures, including biopolymers of complex topology in dense active suspensions.

Received 30th January 2024,
Accepted 7th April 2024

DOI: 10.1039/d4sm00144c

rsc.li/soft-matter-journal

1 Introduction

Active matter is composed of small units, each of which converts their internal energy into directed motion.[1–3] The nature of active matter is described by non-thermal fluctuations, broken detailed balance, and violation of the dissipation–fluctuation relation, maintaining the system out of equilibrium. This allows some fascinating applications and behaviors over its passive counterpart, for example, transportation of cargo and efficient delivery to a target site *in vivo* as well as *in vitro*.[4,5] The presence of active and passive components is an important aspect of living systems.[6–10] The motility of microorganisms in such systems is crucial for nutrient biomixing and maintaining ecological balance in aqueous environments. The enhanced diffusion of a variety of passive particles, such as enzymes, granules, or extracellular products, by cyclic conformational changes in biomolecules such as DNA and RNA is fueled by ATP during the active transcription process. This is essential for the proper functioning of a cell and promotes intercellular signaling and metabolite transport.[11,12] In recent years, there have been a number of studies reported on the statistical mechanics of passive agents in active bath[13–25,29–31] and active agents in the passive bath.[26–28]

Example includes a passive linear semiflexible polymer submerged in a bath of ABPs showing a wide range of transient states in 2D.[32–35] In general, the semiflexible polymer bends due to the activity of bath particles, and ABPs accumulate in the regions of the highest curvature, as has been observed for ABPs in confinement. This leads to hairpin structures for semiflexible polymer that are only temporarily stable, and dissolve and rebuild over time, whereas flexible polymers immersed in the active bath expand monotonically with activity.[16,21–25] Linear flexible polymers composed of active Brownian particles (ABPs) qualitatively demonstrate similar monotonic expansion with activity, albeit to a greater extent.[24,36] While a linear polymer topology was studied before, not much attention has been given to branched and star polymers in an active bath. Star-shaped polymers are polymers in which many arms are connected at one center. Biopolymers of such shapes exist in the form of viruses, which are known as astroviruses.[37] In a few examples from literature, scientists have biologically engineered star-shaped molecules to mimic properties of viruses and studied their dynamics.[38,39] It is also interesting to note

[a] *Department of Chemistry, Indian Institute of Technology Bombay, Mumbai 400076, India. E-mail: rajarshi@chem.iitb.ac.in*
[b] *Institute of Physics and Astronomy, University of Potsdam, Germany. E-mail: rmetzler@uni-potsdam.de*
[c] *Asia Pacific Center for Theoretical Physics, Pohang 37673, Republic of Korea*

† Electronic supplementary information (ESI) available. See DOI: https://doi.org/10.1039/d4sm00144c

that scientists and engineers have begun synthesizing star-shaped polymers which are more efficient for drug delivery due to their tunable properties.[40–44] Some computational studies on star polymers have been performed in passive baths (good and bad solvent),[45] where the authors have studied the conformational changes and dynamics. Additionally, other studies on star polymers are related to their flow-induced translocation through nanopores.[46,47] The investigation of star polymers in an active bath is, however, still largely elusive.

An interesting feature of active matter is collective motion, for example, flocking of birds, swarming of bacteria, and schooling of fish[48–56] *etc.* Such a collective behavior is absent in their passive counterparts. In addition to these natural phenomena, there are some experimental studies in which phase separation appears due to entanglement of active polymer-like worms.[57] An interesting aspect of active systems is that even though particles are repulsive and symmetric (spherical ABPs), phase separation is observed for sufficiently strong active forces and ABP packing fractions. This phenomenon is known as motility-induced phase separation (MIPS).[55,58,59] Here, activity separates the system into dense and dilute regions. In this case, the coexistence boundary is akin to the binodal curve of an equilibrium fluid, with Péclet number (Pe) serving as the measure of attraction strength. Although the phase separation in this system stems from athermal factors, simulations quenched to parameters within the binodal curve exhibit typical phase separation kinetics. Near the binodal, systems encounter a nucleation delay, sometimes necessitating artificial seeding to render phase separation computationally feasible due to its potential duration.[60] Deeper quenching results in spinodal-like decomposition, leading to a coarsening regime characterized by a gradual saturation of the mean cluster size.[55] A similar phase behavior is observed in the case of starvation-induced fruiting body formation in *Myxococcus xanthus*, where a phase separation process is initiated by cells adjusting their motility over time. This phase separation phenomenon is also influenced by cell density and is characterized by Pe, which encompasses cell motility through both speed and reversal frequency. Their findings suggest that *M. xanthus* effectively employs a self-driven nonequilibrium phase transition, providing control at the individual cell level.[61] Furthermore, by adjusting certain physical parameters of colloidal particles, such as their softness and chirality, one can effectively alter the kinetic and critical values associated with phase separation. For instance, increasing the softness of colloidal particles tends to shift critical values towards higher ranges.[55,62–66] In addition to these discussions, the inclusion of torque in ABPs, as well as topological constraints such as connecting them in a ring, also disrupts conventional MIPS, instead exhibiting micro-phase separation.[65,67]

At high packing fractions, mixtures of active and passive particles show even more fascinating effects.[68–71] Simulations of a two-dimensional binary mixture of active and passive particles yield phase separation for sufficiently strong activities. The formation of a dense cluster of passive particles covered by layers of active particles[72–75] is observed here. Phase separation of passive particles is also found due to the difference in temperatures,[76–78] but the underlying mechanism is not the same. The micron-size polymer behavior in the dense active bath after phase separation shows intriguing results. This gives rise to a different set of conformational and dynamical properties of the polymer in comparison to its low-packing fraction counterparts (homogeneously distributed active systems). For example, a flexible polymer shrinks instead of expanding with activity and has a caged-like motion because of the formation of a cluster in the nearby region.[79] The investigation of the different conformations adopted by the star polymer compared to the linear polymer in a highly dense active bath will be another interesting aspect to study.

Using computer simulations in 2D, we explore the structure and dynamics of a star polymer made up of passive monomers immersed in a bath of ABPs. We study the conformational and dynamical changes as a function of activity and packing fraction. We also investigate the associated MIPS and how the presence of a passive star polymer affects this phenomenon. Our calculations suggest that at high packing fractions, the presence of the star polymer affects the growth of cluster formation but not the critical activity for phase separation. On the contrary, for relatively low area-fractions, both nucleation and cluster growth are affected. Clusters grow in the vicinity of the star polymer and experience a trapped motion similar to ABPs in the dense region. The topological constraints and clustering in the neighborhood of the star polymer give rise to interesting conformational changes. We observe the shrinking of the star polymer arms with increasing activity, along with the formation of a short-lived hairpin-like structure. We also see the pairing of two arms of the star polymer, where one arm is largely separated.

This paper is organized as follows. In Section 2, we describe the model and simulation details. Results are presented and discussed in Section 3 followed by the conclusions in Section 4.

2 Model and simulation details

We carry out coarse-grained computer simulations for a passive star polymer (with three arms, each arm has 20 monomers of diameter σ connected with a central bead) embedded in a bath of ABPs in two dimensions. To set up the system, we fix the passive star polymer in a square box of length 120σ (where σ is the diameter of the polymer bead) populated with ABPs. A schematic of our system is shown in Fig. 1. We have fixed the packing fraction of the bath by taking the number N_{ABP} = 11 007 of ABPs for ϕ = 0.6, N_{ABP} = 9171 for ϕ = 0.5, and N_{ABP} = 7338 for ϕ = 0.4. The box length is fixed at 120σ. Here, the packing fraction is defined as:

$$\phi = \frac{N_{\mathrm{ABP}} A_{\mathrm{ABP}}}{120\sigma \times 120\sigma}, \tag{1}$$

where N_{ABP} is the number of ABPs and $A_{\mathrm{ABP}} = \pi\left(\frac{\sigma}{2}\right)^2$ is the area of a single ABP.

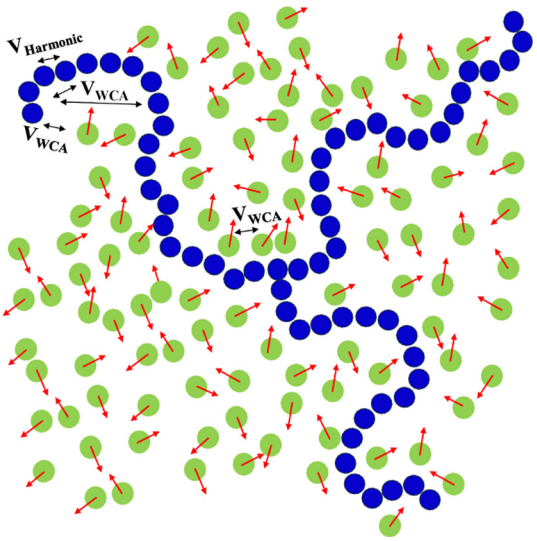

Fig. 1 A schematic depiction of the model system (not to scale): a single star polymer with three arms (blue) is immersed in a dense bath of ABPs (green). The red arrows show the instant direction of ABPs. The pairwise non-bonded interactions among the beads of the polymer and to the ABPs, as well as among the ABPs are WCA, which are shown as double headed arrows. In addition, there is a harmonic interaction to connect the neighbouring beads of polymer.

We apply periodic boundary conditions in all directions throughout our simulations. The beads of the star polymer are connected by harmonic springs with the harmonic potential

$$V_{\text{Harmonic}}(r_{ij}) = k\frac{1}{2}\left(\left(|r_i - r_j|\right) - l_0\right)^2. \quad (2)$$

Here k is the spring constant, $|r_i - r_j|$ is the distance between the i^{th} and j^{th} particles which are connected, and l_0 is the equilibrium bond length. The self-avoidance of the chain beads with ABPs, as well as against each other is modeled by the repulsive part of the Lennard-Jones (LJ) potential, which is also known as the Weeks–Chandler–Andersen (WCA) potential,

$$V_{\text{WCA}}(r_{ij}) = \begin{cases} 4\varepsilon_{ij}\left[\left(\frac{\sigma_{ij}}{r_{ij}}\right)^{12} - \left(\frac{\sigma_{ij}}{r_{ij}}\right)^{6}\right] + \varepsilon_{ij}, & \text{if } r_{ij} < 2^{1/6}\sigma_{ij}, \\ 0, & \text{otherwise} \end{cases} \quad (3)$$

where r_{ij} is the separation between the ith and jth particle, and ε_{ij} is the strength of the interaction with an effective interaction diameter of $\sigma_{ij} = \frac{\sigma_i + \sigma_j}{2}$. In what follows, we measure the length in units of σ and the energy in units of the thermal energy k_BT, where k_B is the Boltzmann constant, and T is the temperature of bath. We set the model parameters to $\sigma_{ij} = \sigma$, $l_0 = \sigma$, $k = 5 \times 10^3$, and $\varepsilon_{ij} = 1$.

The dynamics of the position $r_i(t)$ of the ith particle is described by the Langevin equation,

$$m\frac{\mathrm{d}^2\mathbf{r}_i(t)}{\mathrm{d}t^2} = -\gamma\frac{\mathrm{d}\mathbf{r}_i}{\mathrm{d}t} - \sum_j \nabla V(\mathbf{r}_i - \mathbf{r}_j) + \mathbf{f}_i(t) + F\mathbf{n}(\theta_i). \quad (4)$$

In the overdamped limit, the inertial term $m\frac{\mathrm{d}^2\mathbf{r}_i(t)}{\mathrm{d}t^2}$ is negligibly small compared to the drag force $\gamma\frac{\mathrm{d}\mathbf{r}_i}{\mathrm{d}t}$, where γ is the friction coefficient. To ensure the system is practically overdamped, we have taken a very high value of $\gamma = \frac{1}{10^{-3}}$, m is the mass of the particles. $V(r_i - r_j)$ is the total pairwise interaction potential and is described as $V(r_i - r_j) = V_{\text{WCA}}(r_i - r_j) + V_{\text{Harmonic}}(r_i - r_j)$. The thermal force $\boldsymbol{f}_{i\alpha}(t)$ is the α (not to be confused with the scaling exponent defined later) component of the Gaussian white noise acting on particle i, with zero mean and variance $\langle \boldsymbol{f}_{i\alpha}(t')\boldsymbol{f}_{j\beta}(t'')\rangle = 2\gamma k_B T\delta_{\alpha\beta}\delta_{ij}\delta(t' - t'')$, where, δ_{ij} is the Kronecker delta and $\delta(t)$ is the Dirac delta function.[80] The ABPs are simulated as disks of diameter σ moving under the action of a constant force F along a predefined orientation vector

$$\mathbf{n}(\theta_i) = \{\cos(\theta_i), \sin(\theta_i)\}. \quad (5)$$

$F\mathbf{n}$ is the active force that drives the system out of equilibrium, and F is the active force amplitude directly related to the ABPs propulsion strength. It can be expressed in terms of the Péclet number (Pe) and the particle velocity (v) as

$$\mathrm{Pe} = \frac{v\sigma}{D} = \frac{F\sigma}{k_B T} \quad (6)$$

where Pe = 0 for passive star polymer beads and $\neq 0$ for ABPs.

The orientation (θ_i) of the velocity of the ith ABP is changing as a function of time according to the standard stochastic equation,

$$\frac{\mathrm{d}\theta_i}{\mathrm{d}t} = \sqrt{2D_R} \times \boldsymbol{\eta}(t), \quad (7)$$

where D_R is the rotational diffusion coefficient and $\boldsymbol{\eta}(t)$ is a Gaussian random number with zero mean and unit variance.

All simulations are performed using a Langevin thermostat, and the equation of motion is integrated using the velocity Verlet algorithm in each time step. We initialize the system by placing the star polymer in the center of the bath and relaxing the initial configuration for 10^7 steps. The simulations are carried out for 5×10^8 steps, where the integration time step is considered to be 5×10^{-5} and the positions of the monomers are recorded every 100th step. The simulations are carried out using LAMMPS,[81] a freely available open-source molecular dynamics package.

3 Results

3.1 Characterization of the active bath

3.1.1 Bath of ABPs at ϕ = 0.4. It has been noted in the literature that systems quenched close to the binodal boundary often experience a nucleation delay, which can be prolonged to the extent that artificial seeding becomes necessary to make phase separation computationally accessible.[55] In our investigation, particularly at a packing fraction of $\phi = 0.4$ and Pe = 100, nucleation delay is not kinetically accessible.[55,61] Therefore, we are examining the system at this packing fraction to elucidate

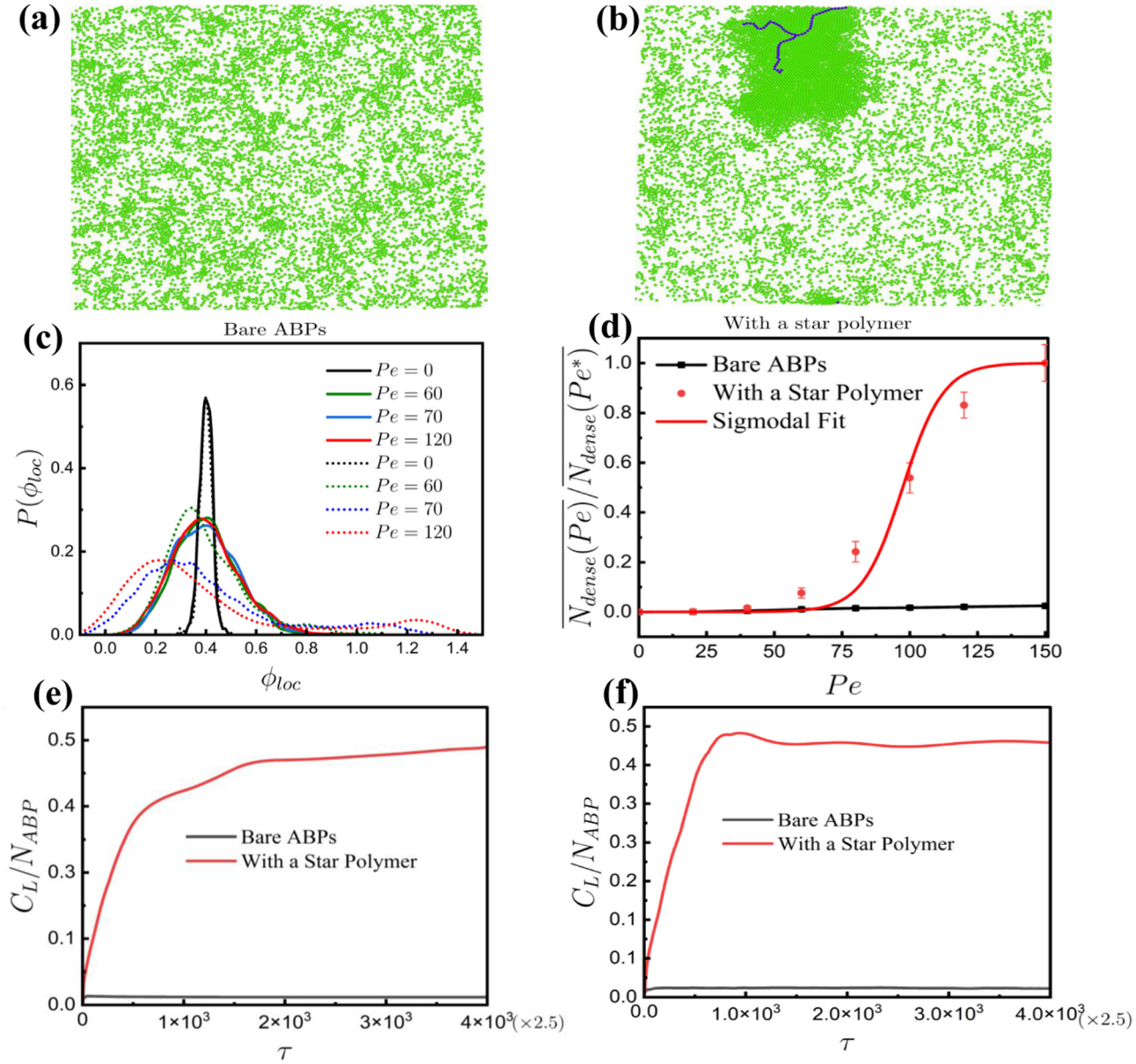

Fig. 2 Snapshots for the last frame of the simulation (Pe = 100, ϕ = 0.4) of the active bath (a) without a star polymer; (b) with a star polymer. Plots at ϕ = 0.4 of (c) local packing fraction distribution in the absence (solids line) and presence of a star polymer (dotted line), (d) $\overline{N_{\mathrm{dense}}(\mathrm{Pe})}\Big/\overline{N_{\mathrm{dense}}(\mathrm{Pe}^*)}$ with activity in the absence of star polymer (black lines), and in the presence of star polymer (red lines), time evolution of C_L/N_{ABP} at (e) Pe = 120, and (f) Pe = 150.

whether the introduction of a flexible elongated object, such as a star polymer may induce a phase separation.

In Fig. 2(a), we present a snapshot of the bath of bare ABPs for the last frame of the simulation at Pe = 100, and ϕ = 0.4. There is no signature of clustering in this scenario. In contrast, with the star polymer under the same parameters and time, profound clustering is evident in the vicinity of the polymer, as shown in Fig. 2(b). To quantify the extent of phase separation, we calculate some physical properties. As we know, during phase separation, ABPs in the bath separate into dilute and dense phases; hence, the calculation of the local area fraction becomes an important property, whose distribution will give two distinct populations (bimodal distribution). We calculate the local area fraction by dividing the area of the box into smaller square bins of side b. The local packing fraction is then given by $\phi_{\mathrm{loc}} = \frac{n\pi(0.5\sigma)^2}{b^2}$, where n is the number of particles in the small bins. The distribution of local area fraction is shown in Fig. 2(c) (solid line). We observe that for bare ABPs, an increase in activity results in longer tails in the distribution instead of bimodality, which rejects the possibility of phase separation. However, on inclusion of the star polymer at the same packing fraction of the bath, bimodality is observed at high Pe, which is prominent for Pe = 120 and ϕ = 0.4 (red dotted line in Fig. 2(c)). To support our results, we calculate the number of ABPs in the dense phase by fixing a

threshold local packing fraction of 0.95, which is the packing fraction at which the region of high packing fraction begins in the distribution. This value is just above the packing fraction of approximately 0.91 for hard particles in a two-dimensional hexagonal packing arrangement. Thus, due to the smaller ε_{ij} value of 1, there is some extent of overlapping between the particles in the dense region. If the particle is in a local packing fraction ≥ 0.95, we consider it to be in the dense region. We plot the relative averaged number $\overline{N_{\mathrm{dense}}(\mathrm{Pe})}\Big/\overline{N_{\mathrm{dense}}(\mathrm{Pe}^*)}$ of particles in the dense phase with activity, where Pe* is the activity at which the size of the cluster saturates. We observe that even with an increased Pe value of 150, the system comprising bare ABPs does not exhibit phase separation and $\overline{N_{\mathrm{dense}}(\mathrm{Pe})}\Big/\overline{N_{\mathrm{dense}}(\mathrm{Pe}^*)}$ is constant with activity as shown in Fig. 2(d) (black line). In the same figure, we observe that the red line changes sigmoidally with activity, corresponding to the bath with the star polymer. The sigmoidal change of $\overline{N_{\mathrm{dense}}(\mathrm{Pe})}\Big/\overline{N_{\mathrm{dense}}(\mathrm{Pe}^*)}$ is the signature of phase separation, supporting the previous statement. The time evolution of the fraction of ABPs in the largest cluster, denoted as $C_{\mathrm{L}}/N_{\mathrm{ABP}}$, where C_{L} represents the number of ABPs in the largest cluster, exhibits an increasing trend followed by saturation at steady state in the presence of the star polymer. Conversely, in the absence of the star polymer, this fraction remains constant, as illustrated in Fig. 2(e) and (f). This proves that at low area fraction, nucleation and coarsening are both facilitated by the inclusion of the star polymer. We observe in Movies S1 and S2 (ESI†) that in the bath of ABPs without the star polymer, there is no stable nucleation center. However, in the presence of the star polymer, a cluster nucleates in the vicinity of the star polymer and grows with time.

3.1.2 Bath of ABPs at ϕ = 0.6. In the case of high packing fraction ϕ = 0.6, beyond a critical activity, the system is in the deep spinodal-like region of phase boundary. In this case, there are many small clusters bloom slowly converging to a large cluster (coarsening).[55,61,64,82] As is demonstrated in Fig. 3(a), there are two distinct phases which are also found on the inclusion of the star polymer (Fig. 3(b)). However, in the latter case, the largest cluster is in the vicinity of the star polymer in Fig. 3(b). To quantify the influence of the star polymer at this packing fraction, we calculate related physical properties in the specified activity range (Pe = 0...150) as discussed in the previous section. We validate the presence of a phase separation by studying the bimodality of the local packing fraction distribution after reaching a critical Péclet number (Pe = 70), indicating the coexistence of liquid and gas phases, see Fig. 3(c). Notably, the behavior of the local area fraction remains relatively unchanged with the inclusion of the star polymer (solid lines are for the bare ABP bath and dotted lines are for the ABP bath with the star polymer in Fig. 3(c)). A similar trend is observed for the number of particles within the dense phase. Fig. 3(d) illustrates the sigmoidal change in the relative averaged number of particles in the dense phase $\overline{N_{\mathrm{dense}}(\mathrm{Pe})}\Big/\overline{N_{\mathrm{dense}}(\mathrm{Pe}^*)}$ with activity, confirming the occurrence of phase separation. However, the inclusion of star polymer does not exhibit significant changes in this plot.

We have additionally computed the ratio $C_{\mathrm{L}}/N_{\mathrm{ABP}}$ of ABPs in the largest cluster relative to N_{ABP}, to examine the impact of the presence of the star polymer, as illustrated in Fig. 3(e) and (f). Our observations reveal that in the presence of the star polymer, the cluster tends to grow in the vicinity of the star polymer, as evident in Movies S3 and S4 (ESI†), as well as in Fig. 3(a) and (b). The rate of cluster growth is initially accelerated with the inclusion of the star polymer, reaching saturation at a similar cluster size over an extended period. Notably, we find that the effect of the star polymer diminishes at high activity, as the activity surpasses the effect of a stable nucleation around the star polymer.

To understand the arrangement of ABPs after phase separation, we examine Voronoi diagrams[83] in a magnified part of the cluster region. The hexatic arrangement of particles in the dense region is evident in Fig. 4(a), while Fig. 4(b) displays randomly arranged particles in the dilute region. Notably, ABPs in the dense region near the star polymer exhibit a disturbed hexatic pattern (Fig. 4(c)). This hexatic arrangement is further confirmed by the radial distribution function, showing a characteristic splitting near 2σ after phase separation (Fig. S1 see the ESI†). As we see from the Voronoi diagram in Fig. 4(a), particles are arranged in hexatic patterns in dense regions of MIPS. Therefore, it can be concluded that the extent of the hexatic pattern increases as the cluster grows. The extent of the hexatic pattern is quantified through the local hexatic order parameter $\phi_{6i} = \frac{1}{N_{\mathrm{v}}}\sum_{j\varepsilon N_{\mathrm{v}}} \mathrm{e}^{6i\theta_{ij}}$ followed by the global hexatic order parameter, $\psi_6 = \left\langle \left| \frac{1}{N_{\mathrm{ABP}}} \sum_{i=1}^{N_{\mathrm{ABP}}} \phi_{6i} \right| \right\rangle$. Here, N_{v} is the number of ABPs in the surrounding of a particle of interest, and θ_{ij} is the angle between the ith and the jth particle from a reference axis. The sigmoidal change of the relative averaged-global hexatic order parameter $\overline{\psi_6(\mathrm{Pe})}\Big/\overline{\psi_6(\mathrm{Pe}^*)}$ with activity confirms the phase transition in Fig. S2 (see the ESI†).

Even though the cluster is stable, there is an ongoing exchange of ABPs between dense and dilute regions. This dynamic property is quantified by assessing the residence time of ABPs within the dense region. To accomplish this, we define a box with a side length of 20σ in close proximity to the center of mass of the star polymer, where the cluster undergoes growth. The duration for which a particle remains within this designated box is then determined. Under conditions of zero activity (Pe = 0), as depicted in Fig. 5(a), the residence time distribution of ABPs aligns seamlessly with the exponential decay function $P(t_{\mathrm{res}}) = (a/t_{\mathrm{res}\star})\exp(-t_{\mathrm{res}}/t_{\mathrm{res}\star})$ (solid line in Fig. 5(a)), with fitting parameters provided in ESI,† Table S2. The perfect fit of the data to the exponential function yields a residence time attributable to simple Brownian motion. The inserted plot in Fig. 5(a) illustrates the distribution on a log–log scale, demonstrating a nearly linear decay. However, at high activity levels (Pe = 120), where phase separation occurs, the distribution of residence time exhibits a bi-exponential decay.

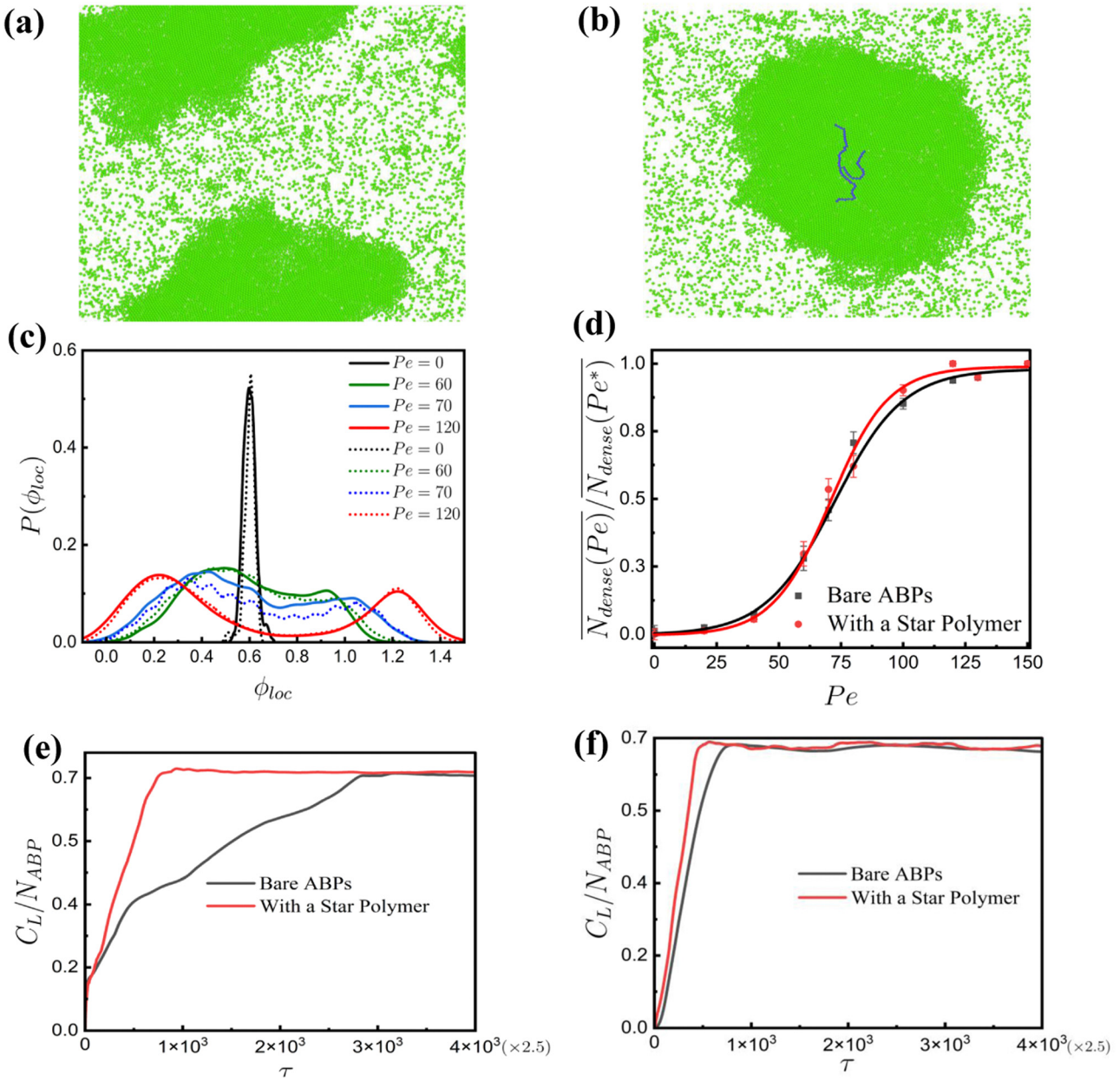

Fig. 3 Snapshots for the last frame of the simulation (Pe = 100, ϕ= 0.6) of the active bath (a) without a star polymer; (b) with a star polymer. Plots at ϕ = 0.6 of (c) local packing fraction distribution in the absence (solids line) and presence of a star polymer (dotted line), (d) $\overline{N_{\mathrm{dense}}(\mathrm{Pe})}\Big/\overline{N_{\mathrm{dense}}(\mathrm{Pe}^*)}$ with activity in the absence of star polymer (black lines), and in the presence of star polymer (red lines), time evolution of C_L/N_{ABP} at (e) Pe = 120, and (f) Pe = 150.

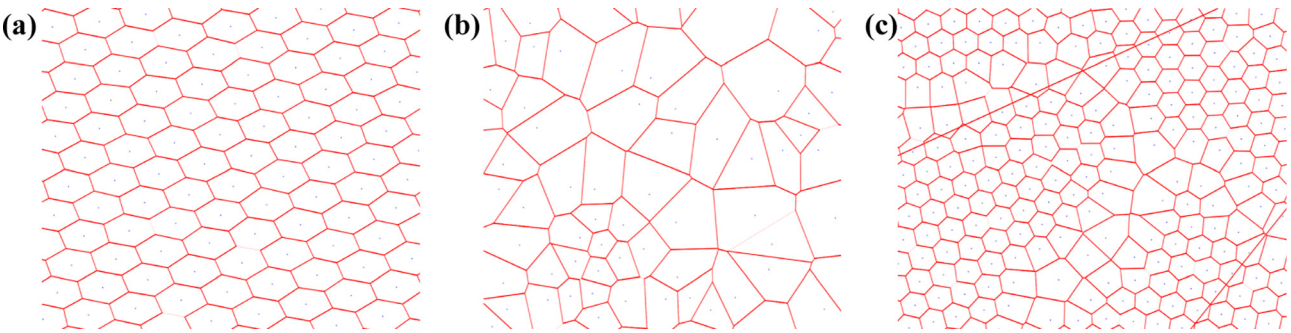

Fig. 4 Magnified part of Voronoi's diagram for particles arranged in (a) cluster region, (b) dilute region, and (c) in the vicinity of the star polymer, where ϕ = 0.6.

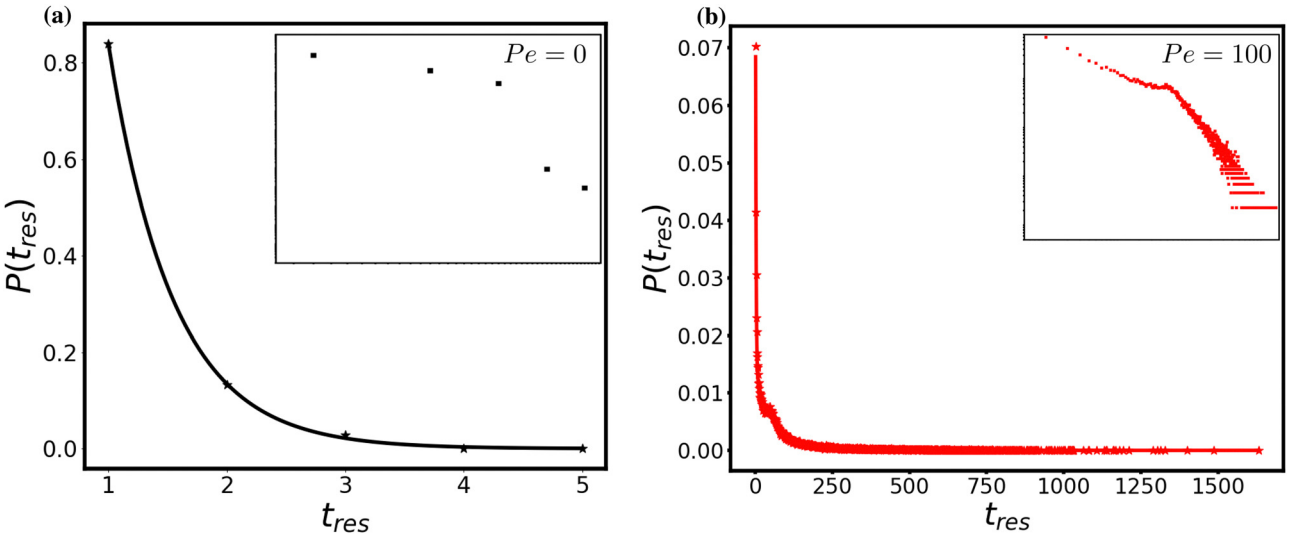

Fig. 5 Distribution of the residence time of ABPs in the vicinity of polymer for (a) Pe = 0, where the solid line is an exponential fit to the data, (b) Pe = 120, here the solid line is a biexponential fit to the data. Inserted plots are distribution on (log–log) scale corresponding to given Pe.

This is evident in the excellent fit of the data to the bi-exponential function $P(t_{res}) = (c/t_{res1})\exp(-t_{res}/t_{res1}) + (d/t_{res2})\exp(-t_{res}/t_{res2})$ (solid line in Fig. 5(b)). The fitting parameters from this equation yield two residence times, t_{res1} and t_{res2}, as given in ESI,† Table S2. Similarly, the inserted plot in Fig. 5(b) depicts the distribution on a log–log scale, providing a visual representation of the bi-exponential behavior. This bi-exponential decay is attributed to the clustering and exchange of particles between the cluster and its surroundings.

To illustrate the kinetics and the phase behavior of MIPS in the presence of a passive star polymer, we calculate the time evolution of the dense fraction of ABPs for packing fractions of $\phi = 0.4$, 0.5, and 0.6 at Pe = 100, and $\varepsilon_{ij} = 1$ as shown in Fig. 6. For bare ABPs at $\phi = 0.4$, the system is close to a region where the nucleation delay time is so high that accessing phase separation without artificial nucleation seeds becomes challenging (black line in Fig. 6(a)). Generally, the inclusion of star polymer provides a stable nucleation center, accelerating the system's attainment to steady state (red line in Fig. 6(a)). Upon increasing the packing fraction to $\phi = 0.5$ for bare ABPs at the same activity, the nucleation delay is accessible in the given range of simulation time and a nucleation event, though delayed quickly, leads to a steady state (black line in Fig. 6(b)), here also inclusion of a star polymer reduces the nucleation delay time (red line in Fig. 6(b)). It is evident from 6a and b that in the presence of the star polymer, the time evolution of the dense fraction shows minimal nucleation delay, followed by growth and saturation to a steady state. At $\phi = 0.6$ and for the same activity, the system resides in the spinodal-like region of the phase boundaries, and the spinodal-like decomposition leads to coarsening that slowly evolves toward a steady state (see Fig. 6(c)). It is also evident from Fig. 6(c) that at $\phi = 0.6$, there is

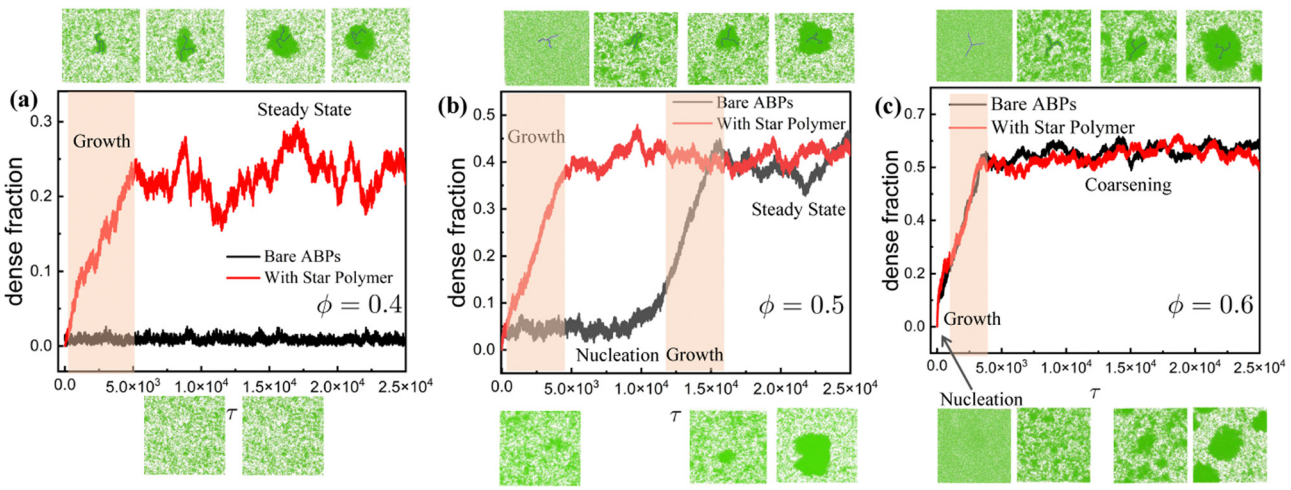

Fig. 6 Time evolution of dense fraction of ABPs at Pe = 100 and (a) $\phi = 0.4$, (b) $\phi = 0.5$, and (c) $\phi = 0.6$. Here black solid lines are for the systems with bare ABPs and red lines are for the systems with ABPs and star polymer.

no effect of the polymer inclusion on the time evolution of the dense fraction, as indicated by the black and red lines merging. This merging occurs because nucleation delay has no effect in this case. These observations illustrate that star polymer facilitates nucleation for cluster growth at low packing fraction without altering the phase behavior.

3.2 Properties of the star polymer (ϕ = 0.6)

The conformational changes of the polymer have a significant impact on the dynamics of polymers in crowded media when subjected to activity.[28,84] In the active bath, the polymer properties strongly depend on the concentration of the ABPs as well as the topology of the polymer. In a medium with a lower packing fraction (when ABPs are distributed homogeneously in the bath), a linear polymer bends and the active particles accumulate in the curvature,[22] which drives the polymer in the same direction. However, in the case of high concentrations when the phase separation of the bath occurs, the properties will be different. In these phase-separated and homogeneous dense media, the dynamical and conformational behavior of the linear polymer is different; it collapses, expands, and localizes in the dense or dilute region of the medium depending on activity.[79] The addition of topological constraints provides further complexities in properties. To investigate these behaviors, we calculate the associated physical quantities.

3.2.1 Dynamics of the star polymer. We investigate the dynamics of the flexible star polymer in a bath of ABPs at ϕ = 0.6. The star polymer switches between several conformations due to the presence of the dense active bath, topological constraints, and phase separation, leading to frustrated dynamics of the star polymer. To explain this, we track the center of mass position of the star polymer (r_{COM}) and calculate the time-averaged $\overline{\delta r_{\mathrm{COM}}{}^2(\tau)} = \frac{1}{T_{\max}-\tau}\int_0^{T_{\max}-\tau}[r_{\mathrm{COM}}(t+\tau)-r_{\mathrm{COM}}(t)]^2\mathrm{d}t$ followed by ensemble-averaged mean-squared displacement $\left\langle\overline{\delta r_{\mathrm{COM}}{}^2(\tau)}\right\rangle = \frac{1}{N}\sum_{i=1}^{N}\overline{\delta r_i^2(\tau)}$ over N different trajectories (Fig. 7(a)). The mean-squared displacement, $\left\langle\overline{\delta r_{\mathrm{COM}}{}^2(\tau)}\right\rangle$, for Brownian motion grows linearly with time, but if the dynamics is anomalous, then $\left\langle\overline{\delta r_{\mathrm{COM}}{}^2(\tau)}\right\rangle \propto \tau^{\alpha}$ (subdiffusion) and $\alpha(\tau) > 1$ (superdiffusion). Initially, in the passive case (Pe = 0), the star polymer's center of mass dynamics is diffusive. Upon inclusion of activity, the results show that the initial dynamics is subdiffusive, which becomes superdiffusive at intermediate times, ultimately crossing over to diffusive dynamics at very long times. The inclusion of activity facilitates clustering in the proximity of the star polymer, and the dynamics becomes subdiffusive over an early period of time. The extent of subdiffusion increases with increasing activity, reflected in the crossing of $\left\langle\overline{\delta r_{\mathrm{COM}}{}^2(\tau)}\right\rangle$ at a shorter time. To quantify the degree of deviation from the diffusive behavior, we calculate the scaling exponent α, defined as $\alpha(\tau) = \frac{\mathrm{d}\log\left(\left\langle\overline{\delta r_{\mathrm{COM}}{}^2(\tau)}\right\rangle\right)}{\mathrm{d}\log\tau}$. In Fig. S3 (see the ESI†) we find that with increasing activity, $\alpha(\tau)$ decreases early in time. The activity does not have a profound effect on the dynamics of the star polymer at the phase separation because of the formation of the largest cluster and trapping around the star polymer that minimizes the effect of activity. This behavior (trapping) is similar to the dynamics of ABPs in the cluster. To confirm our hypothesis, we analyze the $\left\langle\overline{\delta r_i^2(\tau)}\right\rangle$ of ABPs that reside for a longer duration within the boundary of 10σ from the center of mass of the star polymer. The results also reveal that the dynamics is initially subdiffusive. For trapped ABPs, $\alpha(\tau)$ at shorter times has value $\approx \frac{1}{2}$ which is consistent with other studies on MIPS, as shown in (Fig. 7(b)).

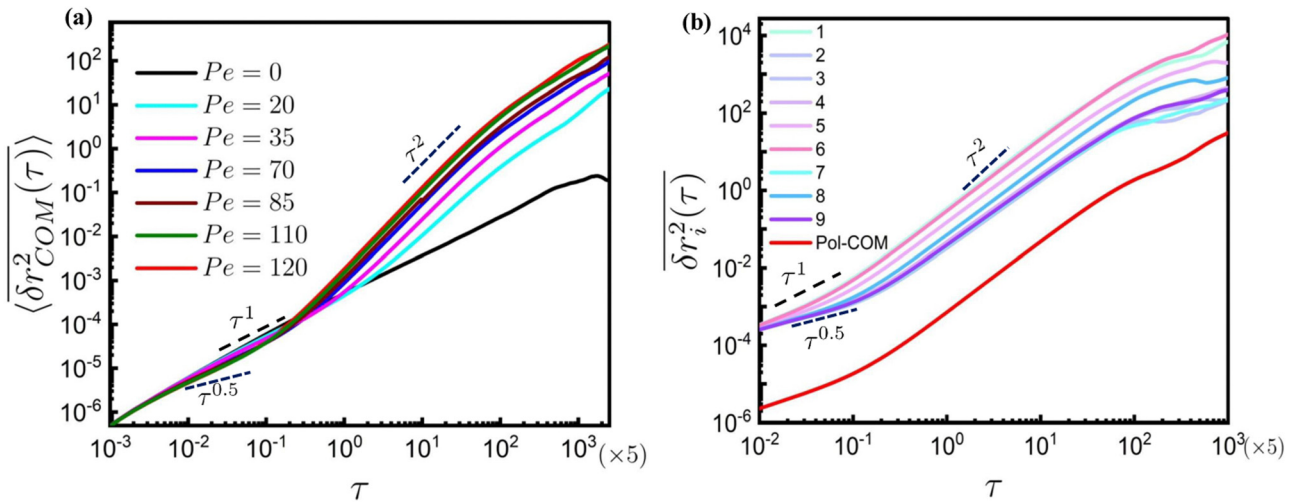

Fig. 7 log–log plot of $\left\langle\overline{\delta r_{\mathrm{COM}}{}^2(\tau)}\right\rangle$ *vs.* τ at ϕ = 0.6 for the (a) center of mass of the star polymer for different activities and (b) ABPs along with the centre of mass (COM) of the star polymer at Pe = 120. In the legend of panel (b), the number stands for the residence time in the vicinity of the star polymer; 9 means that the particle has a long residence time; and 1 means small.

3.2.2 Conformational changes of the star polymer. To study the conformational changes of the star polymer with activity and packing fraction of the bath, we mainly discuss the distance or proximity of two tagged monomers from each other and the distribution of the star polymer beads from their center of mass position. In general, linear flexible polymers expand with activity[21,22,24,25] for low ABP concentrations. However, in our case, due to topological constraints and clustering near the star polymer, each arm of the star polymer shrinks. We begin our analysis by measuring the average squared center-to-end distance $\left\langle \overline{R_{\mathrm{end}}^2} \right\rangle = \left\langle \frac{1}{T_{\max}} \sum_{t=0}^{T_{\max}} \left(R_t^{\mathrm{c}} - R_t^{\mathrm{term}}\right)^2 \right\rangle$ of the arms, where $T_{\max}$ is the total simulation time, R_t^{c} is the position of the central bead at time t, R_t^{term} is the position of the terminal beads of the arm, and $\langle \cdots \rangle$ corresponds to averaging over different trajectories followed by averaging over the three arms. The $\langle R_{\mathrm{end}}{}^2 \rangle$ of each of the star polymer arms changes non-monotonically with activity. Initially, with increasing activity, it decreases, but for very high values, it again starts to increase, which is shown in Fig. 8(a). To support these observations, we calculate the gyration tensor for each arm of the star polymer,

$$S = \frac{1}{N_{\mathrm{beads}}} \begin{pmatrix} \sum_i (x_i - x_{\mathrm{com}})^2 & \sum_i (x_i - x_{\mathrm{com}})(y_i - y_{\mathrm{com}}) \\ \sum_i (x_i - x_{\mathrm{com}})(y_i - y_{\mathrm{com}}) & \sum_i (y_i - y_{\mathrm{com}})^2 \end{pmatrix} \tag{8}$$

where, x_{com} and y_{com} are the coordinates of the center of mass position of the particular arms and $N_{\mathrm{beads}} = 20$ is the number of beads in each arms. Transformation to the principal axis system is carried out by diagonalizing the gyration tensor S; $S = \mathrm{diag}(\lambda_1, \lambda_2)$. The first invariant of S gives the value of squared radius of gyration, $\mathrm{Tr}S = \lambda_1 + \lambda_2 = R_g{}^2$. We average this quantity over time, arms as well as different trajectories. The averaged relative squared radius of gyration $\left\langle \overline{R_g^2(\mathrm{Pe})} \right\rangle / \left\langle \overline{R_g^2(\mathrm{Pe}=0)} \right\rangle$ behaves similarly with activity as the squared end-to-end distance, shown in Fig. 8(b). The asphericity in 2D is defined as $\mathrm{Asp} = \frac{(\lambda_1 - \lambda_2)^2}{(\lambda_1 + \lambda_2)^2}$ and provides information about the anisotropy in the structure of the arms. If $\lambda_1 = \lambda_2$, the asphericity becomes zero which refers to a circular structure. On the contrary, if one component has zero value, the asphericity becomes 1 and refers to a rod-like structure. We find here that the relative averaged (averaged over each arm, time, and different trajectories) asphericity $\left\langle \overline{\mathrm{Asp(Pe)}} \right\rangle / \left\langle \overline{\mathrm{Asp(Pe=0)}} \right\rangle$ follows the same trend with activity (Fig. 8(c)) as in both the previous quantities $\left\langle \overline{R_{\mathrm{end}}{}^2(\mathrm{Pe})} \right\rangle / \left\langle \overline{R_{\mathrm{end}}{}^2(\mathrm{Pe}=0)} \right\rangle$ and $\left\langle \overline{R_g^2(\mathrm{Pe})} \right\rangle / \left\langle \overline{R_g^2(\mathrm{Pe}=0)} \right\rangle$. Here, all results show that with increasing activity, the star polymer shrinks in comparison to the passive bath; and for very high values of activity, it expands again.

Given the complex dynamics observed in our simulations, the average value of the radius of gyration and end-to-end distance of the arms of the star polymer provides only a partial characterization of the system. The key information about the conformation of the star polymer can be extracted from the probability distribution of configurations with a given $R_g{}^2$ and Asp for different activities. Results show that in the passive (Pe = 0) case, the conformation of the star polymer is not going to change and the size distribution is localized at high $R_g{}^2$ and Asp as shown in Fig. 9(a). On increasing the activity, the distribution broadens towards the lower values of Asp and R_g diagonally (Fig. 9(b)). This suggests the shrinking of the arms of the flexible star polymer. If we compare this observation with its linear counterpart in the low packing fraction of ABPs (homogeneously distributed ABPs), it has been found that the flexible polymers swell with activity.[21–23,32] But in our case, due to topological constraints and clustering near the star polymer, it ends up shrinking. After the critical value of activity, when ABPs in the bath get phase-separated into dense and dilute regions, the star polymer localizes in the dense region. As the star polymer is trapped in the dense phase, it adopts a hairpin structure, which is supported by the region of high asphericity and low R_g value in Fig. 9(c) and (d). This region gets more populated if there is a further increase in activity, from Pe = 70 to Pe = 110.

To this point, we have only discussed the changes in individual arms. But we are dealing with a star polymer, which

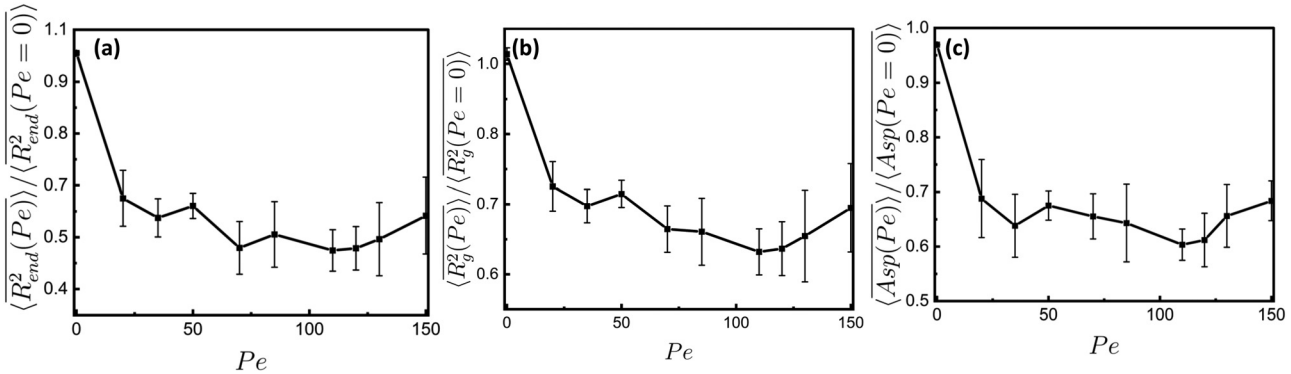

Fig. 8 Relative average squared (a) center-to-end distance $\left\langle \overline{R_{\mathrm{end}}{}^2(\mathrm{Pe})} \right\rangle / \left\langle \overline{R_{\mathrm{end}}{}^2(\mathrm{Pe}=0)} \right\rangle$, (b) radius of gyration $\left\langle \overline{R_g^2(\mathrm{Pe})} \right\rangle / \left\langle \overline{R_g^2(\mathrm{Pe}=0)} \right\rangle$ and (c) relative averaged asphericity $\left\langle \overline{\mathrm{Asp(Pe)}} \right\rangle / \left\langle \overline{\mathrm{Asp(Pe=0)}} \right\rangle$ with activity, at ϕ = 0.6.

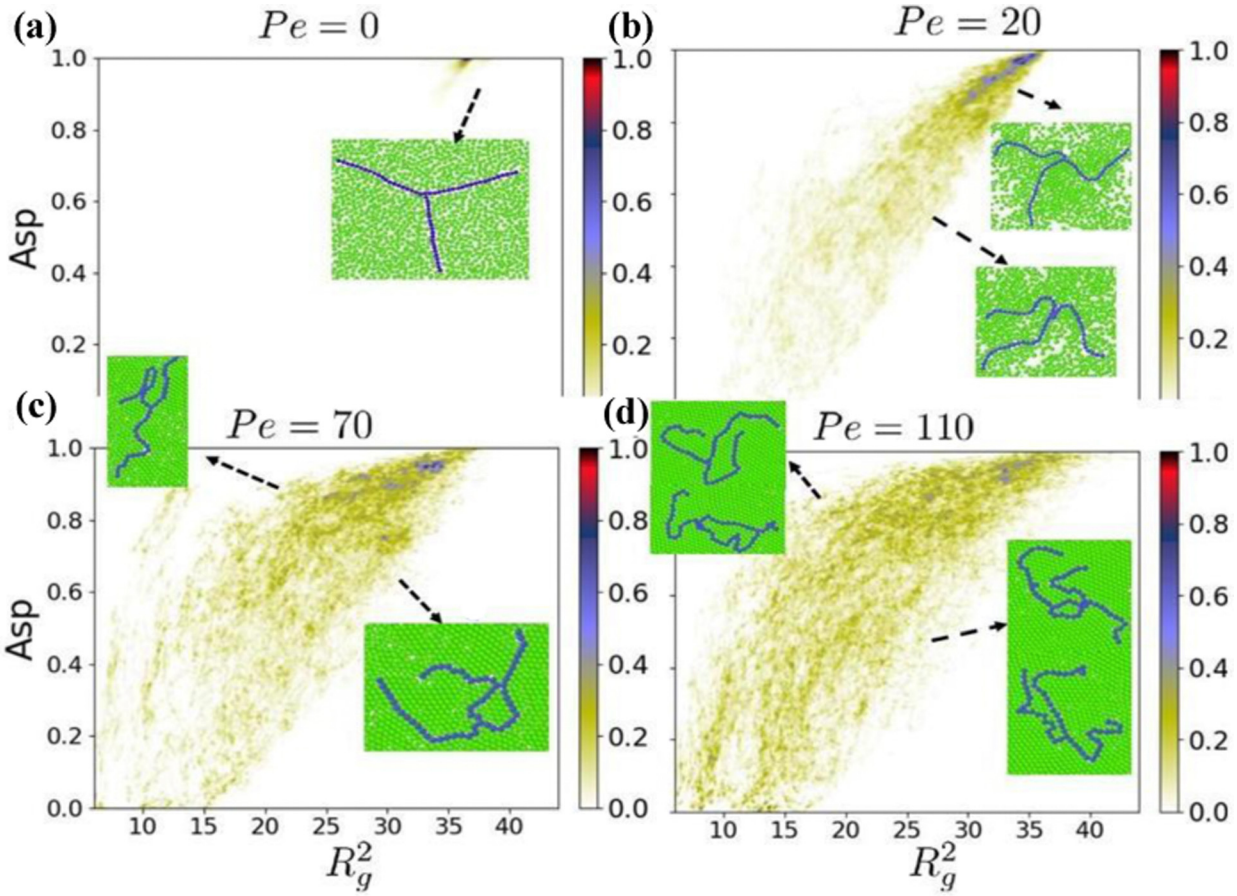

Fig. 9 Colour map obtained for the distribution of radius of gyration R_g and asphericity Asp for all arms of the star polymer. (a) Pe = 0, (b) Pe = 20, (c) Pe = 70 (d) Pe = 120 at ϕ = 0.6. The arrows connect specific locations of the probability distribution to the corresponding conformation snapshots.

has three arms. Hence, to get a complete picture of conformation, it is important to think about arm-to-arm distance. To quantify this, we calculate the squared distances $R_{A_i-A_j}{}^2 = (x_{\mathrm{COM}(i)} - x_{\mathrm{COM}(j)})^2 + (y_{\mathrm{COM}(i)} - y_{\mathrm{COM}(j)})^2$ between the centers of mass of the arms (i, j = 1, 2, 3), which reduce with increasing activity. However, for a very high value of activity, it starts to spread in both directions. Looking at the probability distribution of $R_{A_i-A_j}{}^2$ in Fig. S4 (see the ESI†), we observe that for Pe = 0, we have two distinct peaks corresponding to two combinations, but at intermediate activity values (Pe = 70), all combinations converge to a lower value. For high values (Pe = 130), distribution again becomes wider and attains a peak at larger $R_{A_i-A_j}{}^2$.

Additionally, we show the probability distribution of configurations for different activities at a given $R_{A_i-A_j}{}^2$ and $R_{\mathrm{end}}{}^2$ in Fig. 10. The distribution is localized at a high value of $R_{\mathrm{end}}{}^2$ and two distinct values of $R_{A_i-A_j}{}^2$ for Pe = 0, which resembles the initial conformation of the star polymer (Fig. 10(a)). Turning on the activity, the distribution for Pe = 20 shifts to the lower value of $R_{A_i-A_j}{}^2$ and $R_{\mathrm{end}}{}^2$. At high activities of Pe = 70 and 110, the distributions show a high probability at a low value and high value of $R_{A_i-A_j}{}^2$. These distributions correspond to the conformations shown in Fig. 10(c) and (d), where two arms come close and the third one is largely separated for a short time. This transient pairing of two arms is more evident in Movie S5 (ESI†) at high activity (Pe = 130). In literature it has been shown that at relatively high densities, active hard spheres form a dynamic crystalline structure, creating a robust oscillating bridge between them. This bridge induces a pronounced long-range dynamic repulsion during wetting between walls. However, as the density decreases, this dynamic bridge gradually disintegrates, leading to a fascinating long-range dynamic depletion attraction.[63] Similar phenomena are reported in the literature, where the pairing of two flexible polymers facilitates with increasing activity at low packing fractions.[85] To get a clearer picture, we run the simulation for the ABP system at very small packing fraction (ϕ = 0.06) and find that the depletion force is prominent in this case, effecting prolonged pairing of the two arms (Fig. S5, see ESI†). For the transient pairing of two arms at high activity (Pe = 130), by combining insights from simulations and the literature,[63,85] we conclude that the interplay among topological constraints, clustering, and exertion of high active forces leads to the transient pairing of two arms. In addition to these properties, we calculate the gyration tensor for the total shape of the star polymer, which also follows a similar pattern. The relative averaged radius of gyration,

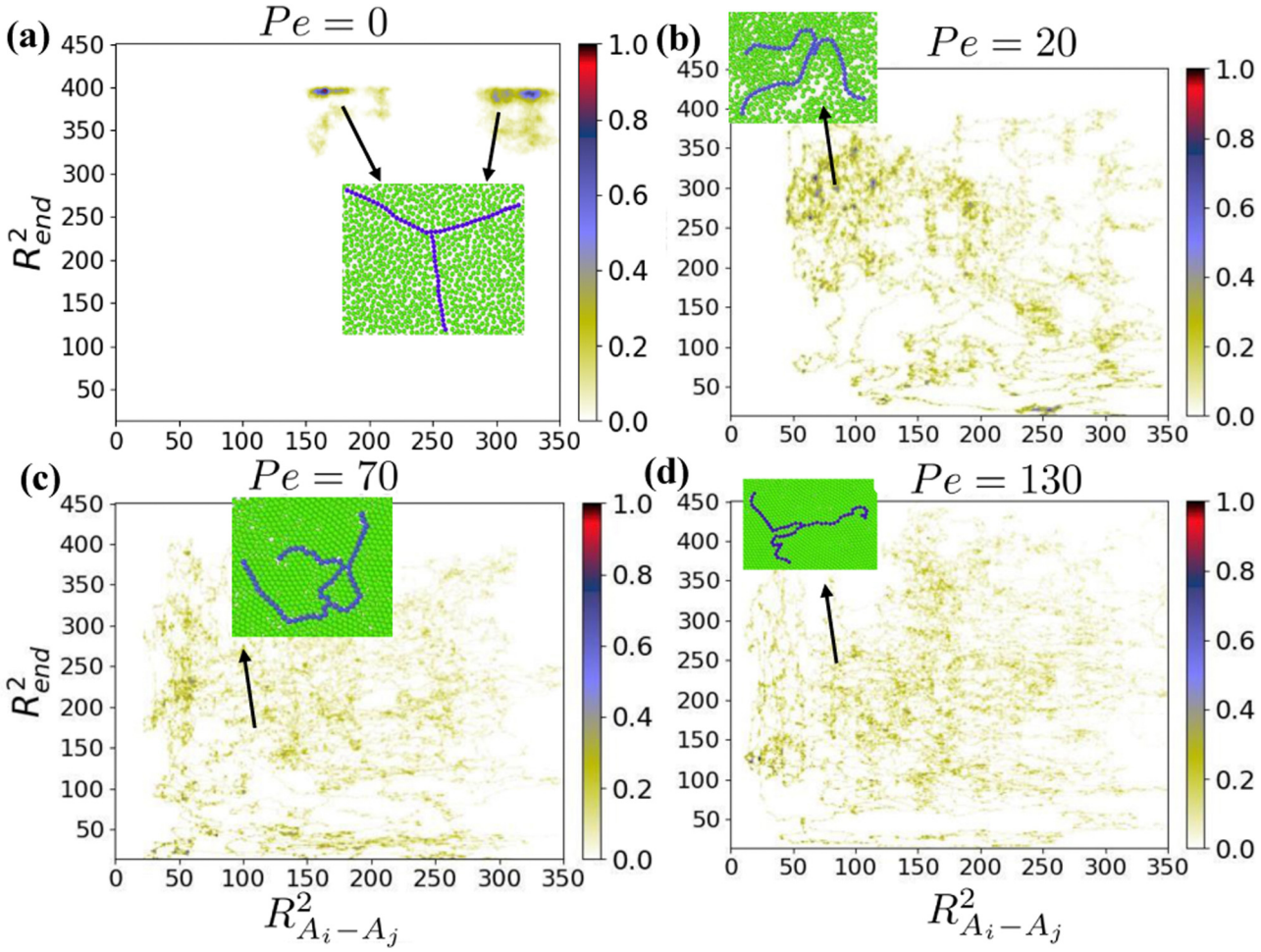

Fig. 10 Colour map obtained for the distribution of the squared arm-to-arm distance $R_{A_i-A_j}{}^2$ for all pairs of arms of the star polymer and squared end-to-end distance $R_{end}{}^2$ for all arms at ϕ = 0.6 and (a) Pe = 0, (b) Pe = 20, (c) Pe = 70, and (d) Pe = 120. The arrows connect specific locations of the probability distribution to the corresponding conformation snapshots.

$\left\langle \overline{R_{g(pol)}{}^2(\mathrm{Pe})} \right\rangle \Big/ \left\langle \overline{R_{g(pol)}{}^2(\mathrm{Pe}=0)} \right\rangle$ decreases with increasing activity, as shown in the Fig. S6 (see the ESI†).

4 Conclusion

Our simulations focus on the behavior of active bath particles in the presence of a star polymer and subsequent MIPS phenomena. The inclusion of a star polymer does not exhibit a significant impact on the behavior of the local area fraction distribution and the relative number of particles in the dense phase with activity during phase separation at a high packing fraction (ϕ = 0.6). However, it does contribute to the enhancement of cluster coarsening properties owing to the presence of slow-moving obstacles. The result is reflected in the time evolution of the largest cluster size, which grows rapidly with the presence of a star polymer in the bath. In this situation, our system is in the spinoidal region where there is no nucleation delay and coarsening is an important factor for the cluster growth which is facilitated in the presence of the star polymer. In contrast, at low packing-fraction (ϕ = 0.4), the presence of star polymer assists both the nucleation as well as cluster growth. This is because at low packing fraction ϕ = 0.4, we are in the region where the nucleation delay is so high that it can not be accessible without artificial seeds, so nucleation is assisted by the presence of the star polymer. To investigate the dynamics of the star polymer, we trace the center of mass position of the star polymer and see that it is similar to the ABPs trapped inside the cluster. This confirms that the star polymer experiences a frustrated dynamics due to the coarsening of the cluster in the surroundings of the star polymer and that the star polymer gets trapped inside the cluster. Here, we try to examine how this clustering affects the conformation of the polymer relative to a passive bath where no clustering occurs. In a passive bath, the star polymer is in its fully swollen conformation. However, upon turning on activity, there is an asymmetric insertion of ABPs, leading to bending of the polymer. In cases of efficient clustering, bent conformations of the polymer are trapped for extended durations, resulting in lower values of $R_g{}^2$ and higher values of Asp in the distribution. Even at very high levels of activity, clustering persists, albeit with faster polymer reconfiguration, thereby yielding a plethora of

additional conformations. It is important to note that clustering is not only confined within the region between the arms but also covers the entire polymer. Consequently, as the cluster grows, both the arms of the polymer and the complete star polymer collapse. This collapse is absent in the passive dense bath. Our choice of star polymer is motivated by the fact that star-shaped polymeric objects have several tunable properties,[40–42] which make them more efficient for drug delivery compared to linear ones. For further insights, we also investigate the arm-to-arm distance for all pairs. We observe that in the passive case, we have two populated states for the arm-to-arm separation and the investigation confirms that with increasing activity, these two states merge to the state with shorter arm-to-arm distance. Beyond a critical value of activity, we see the pairing of two arms, while the third one remains largely separated, reflected in a broad distribution in the arm-to-arm distance. We infer that the phase separation of the bath, high activity and localization of the star polymer in the dense phase provide plenty of transient conformational variants and interesting dynamical behavior in two dimensions. We are hopeful that this study will help scientists and engineers to design polymer-based drug carriers for efficient targeted drug delivery in dense media. Apart from modifying the object suspended in the ABP bath, one can also modify the ABPs themselves. For instance, one can study different versions of active particles[86] as well as heterogeneous ensembles of ABPs.[87,88]

Conflicts of interest

There are no conflicts to declare.

Acknowledgements

R. S. Y. thanks IIT Bombay for the fellowship. R. C. acknowledges SERB, India, project no. MTR/2020/000230 under the MATRICS scheme, and IRCC-IIT Bombay (project no. RD/0518-IRCCAW0-001) for funding. R. S. Y. and S. S. acknowledge Ligesh Theeyancheri for helpful discussions. We acknowledge the SpaceTime-2 supercomputing facility at IIT Bombay for the computing time. R. M. acknowledges the computer facility at the University of Potsdam, Germany and the German Science Foundation (DFG, grant ME 1535/12-1).

References

1 J. Zheng, W. Shen, D. Z. He, K. B. Long, L. D. Madison and P. Dallos, *Nature*, 2000, **405**, 149.
2 Y. Sumino, K. H. Nagai, Y. Shitaka, D. Tanaka, K. Yoshikawa, H. Chaté and K. Oiwa, *Nature*, 2012, **483**, 448.
3 J. T. J. OByrne, Y. Kafri and F. van Wijland, *Nat. Rev. Phys.*, 2022, **4**, 167.
4 D. Patra, S. Sengupta, W. Duan, H. Zhang, R. Pavlick and A. Sen, *Nanoscale*, 2013, **5**, 1273.
5 L. Chen, Y. Wu, H. Wu, J. Li, J. Xie, F. Zang, M. Ma, N. Gu and Y. Zhang, *Acta Biomater.*, 2019, **96**, 491.
6 D. A. Fletcher and P. L. Geissler, *Annu. Rev. Phys. Chem.*, 2009, **60**, 486.
7 D. Bray, *Cell movements: from molecules to motility*, Garland Science, 2000.
8 D. Saintillan, M. J. Shelley and A. Zidovska, *Proc. Natl. Acad. Sci. U. S. A.*, 2018, **115**, 11447.
9 S. Chaki, L. Theeyancheri and R. Chakrabarti, *Soft Matter*, 2023, **19**, 1348.
10 J. I. Prosser, B. J. Bohannan, T. P. Curtis, R. J. Ellis, M. K. Firestone, R. P. Freckleton, J. L. Green, L. E. Green, K. Killham and J. J. Lennon, *et al.*, *Nat. Rev. Microbiol.*, 2007, **5**, 392.
11 A. Caspi, R. Granek and M. Elbaum, *Phys. Rev. Lett.*, 2000, **85**, 5655.
12 C. P. Brangwynne, G. H. Koenderink, F. C. MacKintosh and D. A. Weitz, *J. Cell Biol.*, 2008, **183**, 583.
13 P. Pietzonka and U. Seifert, *J. Phys. A: Math. Theor.*, 2017, **51**, 01LT01.
14 S. Chaki and R. Chakrabarti, *Phys. A*, 2018, **511**, 302.
15 S. Chaki and R. Chakrabarti, *Phys. A*, 2019, **530**, 121574.
16 S. Chaki and R. Chakrabarti, *J. Chem. Phys.*, 2019, **150**, 094902.
17 S. Ye, P. Liu, F. Ye, K. Chen and M. Yang, *Soft Matter*, 2020, **16**, 4655.
18 J. Shea, G. Jung and F. Schmid, *Soft Matter*, 2022, **18**, 6965.
19 K. Goswami and R. Metzler, *Soft Matter*, 2023, **19**, 8802.
20 R. Großmann, L. S. Bort, T. Moldenhawer, M. Stange, S. S. Panah, R. Metzler and C. Beta, *Phys. Rev. Lett.*, 2024, **132**, 088301.
21 S. K. Anand and S. P. Singh, *Phys. Rev. E*, 2020, **101**, 030501.
22 J. Shin, A. G. Cherstvy, W. K. Kim and R. Metzler, *New J. Phys.*, 2015, **17**, 113008.
23 A. Kaiser, S. Babel, B. ten Hagen, C. von Ferber and H. Löwen, *J. Chem. Phys.*, 2015, **142**, 124905.
24 K. Goswami, S. Chaki and R. Chakrabarti, *J. Phys. A: Math. Theor.*, 2022, **55**, 423002.
25 N. Samanta and R. Chakrabarti, *J. Phys. A: Math. Theor.*, 2016, **49**, 195601.
26 R. Majumdar, A. Saha and R. Marathe, *J. Stat. Mech.: Theory Exp.*, 2022, **2022**, 073206.
27 D. Martin, J. O'Byrne, M. E. Cates, É. Fodor, C. Nardini, J. Tailleur and F. Van Wijland, *Phys. Rev. E*, 2021, **103**, 032607.
28 L. Theeyancheri, S. Chaki, T. Bhattacharjee and R. Chakrabarti, *J. Chem. Phys.*, 2023, **159**, 014902.
29 M. S. Aporvari, M. Utkur, E. U. Saritas, G. Volpe and J. Stenhammar, *Soft Matter*, 2020, **16**, 5609.
30 A. Ghosh and N. Gov, *Biophys. J.*, 2014, **107**, 1065.
31 D. Osmanović and Y. Rabin, *Soft Matter*, 2017, **13**, 963.
32 A. Kaiser and H. Löwen, *J. Chem. Phys.*, 2014, **141**, 044903.
33 N. Nikola, A. P. Solon, Y. Kafri, M. Kardar, J. Tailleur and R. Voituriez, *Phys. Rev. Lett.*, 2016, **117**, 098001.
34 S. Mallory, C. Valeriani and A. Cacciuto, *Phys. Rev. E: Stat., Nonlinear, Soft Matter Phys.*, 2014, **90**, 032309.
35 C. J. Anderson, G. Briand, O. Dauchot and A. Fernández-Nieves, *Phys. Rev. E*, 2022, **106**, 064606.

36 T. Eisenstecken, G. Gompper and R. G. Winkler, *Polymers*, 2016, **8**, 304.
37 P. Pérot, M. Lecuit and M. Eloit, *Viruses*, 2017, **9**, 10.
38 A. de la Cotte, C. Wu, M. Trevisan, A. Repula and E. Grelet, *ACS Nano*, 2017, **11**, 10616.
39 A. B. Zavala-Martnez and E. Grelet, *ACS Nano*, 2024, **18**, 281.
40 D.-P. Yang, M. N. N. L. Oo, G. R. Deen, Z. Li and X. J. Loh, *Macromol. Rapid Commun.*, 2017, **38**, 1700410.
41 A. Sulistio, J. Lowenthal, A. Blencowe, M. N. Bongiovanni, L. Ong, S. L. Gras, X. Zhang and G. G. Qiao, *Biomacromolecules*, 2011, **12**, 3477.
42 J. Liu, H. Duong, M. R. Whittaker, T. P. Davis and C. Boyer, *Macromol. Rapid Commun.*, 2012, **33**, 766.
43 S. Biffi, R. Cerbino, F. Bomboi, E. M. Paraboschi, R. Asselta, F. Sciortino and T. Bellini, *Proc. Natl. Acad. Sci. U. S. A.*, 2013, **110**, 15633.
44 D. Liu, S. H. Park, J. H. Reif and T. H. LaBean, *Proc. Natl. Acad. Sci. U. S. A.*, 2004, **101**, 717.
45 T. Taddese, P. Carbone and D. L. Cheung, *Soft Matter*, 2015, **11**, 81.
46 M. Ding, X. Duan and T. Shi, *Soft Matter*, 2016, **12**, 2851.
47 K. Nagarajan and S. B. Chen, *J. Phys. Chem. B*, 2019, **123**, 7919.
48 H. Zhang, A. Be'Er, R. S. Smith, E.-L. Florin and H. L. Swinney, *EPL*, 2009, **87**, 48011.
49 N. C. Darnton, L. Turner, S. Rojevsky and H. C. Berg, *Biophys. J.*, 2010, **98**, 2082.
50 C. Dombrowski, L. Cisneros, S. Chatkaew, R. E. Goldstein and J. O. Kessler, *Phys. Rev. Lett.*, 2004, **93**, 098103.
51 C. W. Wolgemuth, *Biophys. J.*, 2008, **95**, 1564.
52 J. Dunkel, S. Heidenreich, K. Drescher, H. H. Wensink, M. Bär and R. E. Goldstein, *Phys. Rev. Lett.*, 2013, **110**, 228102.
53 M. E. Cates and J. Tailleur, *Annu. Rev. Condens. Matter Phys.*, 2015, **6**, 219.
54 C. Bechinger, R. Di Leonardo, H. Löwen, C. Reichhardt, G. Volpe and G. Volpe, *Rev. Mod. Phys.*, 2016, **88**, 045006.
55 G. S. Redner, M. F. Hagan and A. Baskaran, *Phys. Rev. Lett.*, 2013, **110**, 055701.
56 J. Stenhammar, D. Marenduzzo, R. J. Allen and M. E. Cates, *Soft Matter*, 2014, **10**, 1499.
57 A. Deblais, A. Maggs, D. Bonn and S. Woutersen, *Phys. Rev. Lett.*, 2020, **124**, 208006.
58 Z. Liu, F. Qin, L. Zhu, R. Yang and X. Luo, *Phys. Fluids*, 2020, **32**, 041902.
59 M. R. Shaebani, A. Wysocki, R. G. Winkler, G. Gompper and H. Rieger, *Nat. Rev. Phys.*, 2020, **2**, 199.
60 Y. Du, H. Jiang and Z. Hou, *Soft Matter*, 2020, **16**, 6434.
61 G. Liu, A. Patch, F. Bahar, D. Yllanes, R. D. Welch, M. C. Marchetti, S. Thutupalli and J. W. Shaevitz, *Phys. Rev. Lett.*, 2019, **122**, 248102.
62 M. Sanoria, R. Chelakkot and A. Nandi, *Phys. Rev. E*, 2021, **103**, 052605.
63 R. Ni, M. A. C. Stuart and P. G. Bolhuis, *Phys. Rev. Lett.*, 2015, **114**, 018302.
64 P. Digregorio, D. Levis, A. Suma, L. F. Cugliandolo, G. Gonnella and I. Pagonabarraga, *Phys. Rev. Lett.*, 2018, **121**, 098003.
65 Z. Ma and R. Ni, *J. Chem. Phys.*, 2022, **156**, 021102.
66 A. Torres-Carbajal and F. J. Sevilla, *Phys. Fluids*, 2024, **36**, 027129.
67 L. Theeyancheri, S. Chaki, T. Bhattacharjee and R. Chakrabarti, *Phys. Rev. Res.*, 2024, **6**, L012038.
68 X.-L. Wu and A. Libchaber, *Phys. Rev. Lett.*, 2000, **84**, 3017.
69 M. J. Kim and K. S. Breuer, *Phys. Fluids*, 2004, **16**, L81.
70 D. T. Chen, A. Lau, L. A. Hough, M. F. Islam, M. Goulian, T. C. Lubensky and A. G. Yodh, *Phys. Rev. Lett.*, 2007, **99**, 148302.
71 H. Kurtuldu, J. S. Guasto, K. A. Johnson and J. P. Gollub, *Proc. Natl. Acad. Sci. U. S. A.*, 2011, **108**, 10395.
72 F. Kümmel, P. Shabestari, C. Lozano, G. Volpe and C. Bechinger, *Soft Matter*, 2015, **11**, 6191.
73 J. Stenhammar, R. Wittkowski, D. Marenduzzo and M. E. Cates, *Phys. Rev. Lett.*, 2015, **114**, 018301.
74 A. Wysocki, R. G. Winkler and G. Gompper, *New J. Phys.*, 2016, **18**, 123030.
75 D. R. Rodriguez, F. Alarcon, R. Martinez, J. Ramrez and C. Valeriani, *Soft Matter*, 2020, **16**, 1169.
76 S. N. Weber, C. A. Weber and E. Frey, *Phys. Rev. Lett.*, 2016, **116**, 058301.
77 A. Y. Grosberg and J.-F. Joanny, *Phys. Rev. E: Stat., Nonlinear, Soft Matter Phys.*, 2015, **92**, 032118.
78 J. Smrek and K. Kremer, *Phys. Rev. Lett.*, 2017, **118**, 098002.
79 S. M. Mousavi, G. Gompper and R. G. Winkler, *J. Chem. Phys.*, 2021, **155**, 044902.
80 M. Doi and S. F. Edwards, *The theory of polymer dynamics*, Oxford University Press, 1988, vol. 73.
81 S. Plimpton, *J. Comput. Phys.*, 1995, **117**, 19.
82 J. T. Siebert, F. Dittrich, F. Schmid, K. Binder, T. Speck and P. Virnau, *Phys. Rev. E*, 2018, **98**, 030601.
83 S. Skyum, *Inf. Process. Lett.*, 1991, **37**, 121–125.
84 M. Fazelzadeh, Q. Di, E. Irani, Z. Mokhtari and S. Jabbari-Farouji, *J. Chem. Phys.*, 2023, **159**, 224903.
85 M. Gandikota and A. Cacciuto, *Phys. Rev. E*, 2022, **105**, 034503.
86 P. Romanczuk, M. Bär, W. Ebeling, B. Lindner and L. Schimansky-Geier, *Eur. Phys. J.-Spec. Top.*, 2012, **202**, 1–162.
87 E. Lemaitre, I. M. Sokolov, R. Metzler and A. V. Chechkin, *New J. Phys.*, 2023, **25**, 013010.
88 S. Khadem, N. Siboni and S. Klapp, *Phys. Rev. E*, 2021, **104**, 064615.

